JOURNAL OF SOLID STATE CHEMISTRY 116, 347–354 (1995)

A New "1201" Mercury-Based Cuprate with HgCe Mixed Layers: The Oxide $Hg_{0.4}Ce_{0.5}Cu_{0.1}Sr_{2-x}La_xCuO_{4+\delta}$

A. Maignan, C. Martin, C. Michel, M. Hervieu, and B. Raveau

Laboratoire CRISMAT, CNRS URA 1318, ISMRA et Université de Caen, Boulevard du Maréchal Juin, Caen 14050 Cédex, France

Received June 24, 1994; in revised form November 7, 1994; accepted November 10, 1994

A new "1201" mercury cuprate $Hg_{0.4}Ce_{0.1}Cu_{0.1}Sr_{2-x}La_xCuO_{4+\delta}$ characterized by Hg,Ce and Sr,La mixed layers has been isolated. The electron diffraction study evidences a quadruple cell with regard to the classical 1201 cell resulting in a doubling of the *b* and *c* parameters. The origin of the superstructure is assumed to be due to an ordering between mercury and cerium within the same layers as observed in mixed Hg,Pr layers. XRD calculations and HREM observations support this point of view. Order–disorder phenomena and extended defects observed in these compounds and described and discussed. No superconductivity has been detected.

INTRODUCTION

After the discovery of the mercury-based "1201" superconductor $HgBa_2CuO_{4+\delta}$ (1), attempts were made to synthesize the isostructural compound with strontium. No phase with the formulation $HgSr_2CuO_{4+\delta}$ could be obtained; this could be explained by the low stability of such a phase due to its high oxygen deficiency at the level of the mercury layers. For this reason the possibility of stabilizing the 1201 structure by introducing, besides mercury, a cation with higher valency, but with the same $5d^{10}$ electronic configuration such as Pb(IV) or Bi(V), was considered. Starting from this idea two series of oxides with the 1201 structure were isolated, the 27-K superconductors $Hg_{0.5}Bi_{0.5}Sr_{2-x}La_xCuO_{4+\delta}$ (2) and the 28-K superconductors $Hg_{0.3}Pb_{0.7}Sr_{2-x}La_xCuO_{4+\delta}$ (3). But more surprising is the possibility of stabilizing this structure by introducing praseodymium besides mercury, as demonstrated with the synthesis of the oxide $Hg_{0.4}Pr_{0.6}Sr_{2-x}Pr_xCuO_{4+\delta}$ (3).

Although it belongs to the same 1201 structural family, the Pr–Hg cuprate exhibits a very different behavior from the Bi–Hg or Pb–Hg phases. Contrary to the latter, its structure is not tetragonal but orthorhombic. In fact, it differs from the other 1201 mercury cuprates by an ordering of the mercury and praseodymium ions within the $[Hg_{0.4}Pr_{0.6}O_\delta]_\infty$ layers, leading to a doubling of the *b* parameter (3). This phase differs also from the other 1201 mercury cuprates by the quasi-absence of superconductivity (less than 1%). The ability of praseodymium to induce an ordering phenomenon has already been observed in the mercury-based 1212 structure $Hg_{0.4}Pr_{0.6}Sr_2Ca_{1-x}Pr_xCuO_{6+\delta}$ (4), but in that case superconductivity is enhanced since a sharp transition at 85 K is observed.

This particular behavior of praseodymium, its ability to stabilize the 1201 and 1212 mercury-based cuprates and these ordering phenomena, and the relationships with superconductivity are so far not understood. The main issue deals with the valency of praseodymium in these compounds since both species Pr(III) and Pr(IV) may be involved. From this viewpoint, cerium owing to its ability to exhibit two oxidation states Ce(III) and Ce(IV) should be considered, although very few layered cuprates involving cerium have been synthesized up to date. For this reason the system Hg–Sr–Ce–Cu–O was first explored, and in a second step the system Hg–Sr–La–Ce–Cu–O was investigated. We report herein on a new Hg–Ce cuprate $Hg_{0.4}Ce_{0.5}Sr_{2-x}La_xCu_{1.1}O_{4+\delta}$ with the 1201 structure.

EXPERIMENTAL

The samples were prepared from mixtures of HgO, CeO_2, SrO_2, CuO, and La_2O_3 corresponding to the nominal compositions.

$Hg_{1-y}Ce_ySr_{2-x}Ce_xCuO_z$ (I) $0 \le x \le 0.5$ $0 \le y \le 2/3$.
$Hg_{1-y}Ce_ySr_{2-x}La_xCuO_z$ (II) $0 \le x \le 1.25$ $0 \le y \le 2/3$.

The compounds are heated in evacuated silica ampoules. The temperature is slowly increased up to 800°C in 10 hr, maintained during 30 hr, and then slowly decreased down to 400°C in 10 hr. This thermal process leads to a partial decomposition of CeO_2 and SrO_2 so that an oxygen pressure of several bars is reached during reaction, in order to favor the mixed valency Cu(II)–Cu(III). Different other attempts, varying the temperature from 800 to 880°C and the heating time between 10 hr and several days, did not allow better results to be obtained. The samples were then systematically analyzed by X ray diffraction (XRD),

0022-4596/95 $6.00

electron diffraction (ED) and energy dispersive X ray microanalysis (EDS). The X ray patterns have been registered with a Philips vertical diffractometer (Cu$K\alpha$ radiation) by step scanning in increments of 0.02° (2θ). Lattice constants and structure were refined using a Rietveld method (computer program DBW 3.2 [5]). The ED study was carried out on a JEOL 200CX electron microscope equipped with an eucentric goniometer (±60°). The high resolution electron microscopy (HREM) study was performed with a TOPCON 002B microscope, operating at 200 kV and having a point resolution of 1.8 Å. The magnetic measurements were performed with a SQUID magnetometer at 5 K. Samples for EM study have been gently crushed in alcohol and the grains have been deposited on a holey carbon film (Ni grid); no significant irradiation damage have been detected under the electron beam.

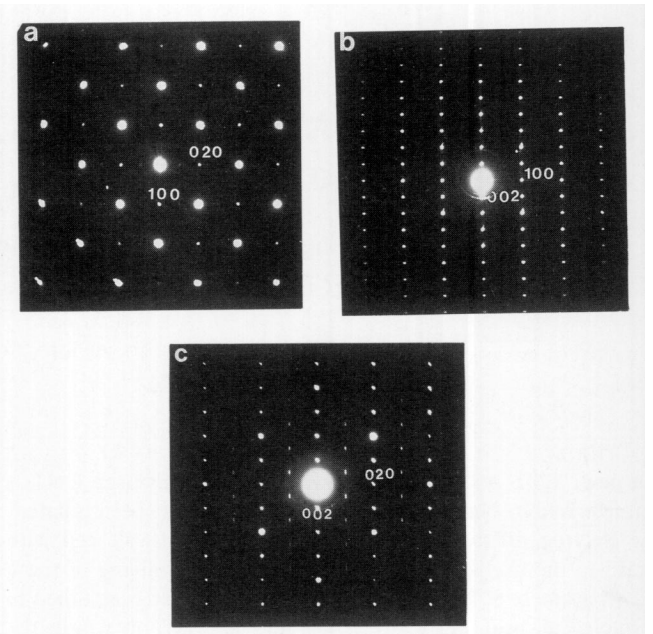

FIG. 1. $Hg_{0.4}Ce_{0.5}Sr_{1.4}La_{0.6}Cu_{1.1}O_{4+\delta}$: (a) [001], (b) [010], and (c) [100] ED patterns.

RESULTS AND DISCUSSION

Homogeneity Range and Structure

Under the experimental conditions described above, no 1201 phase was detected in system (I) that would correspond to the formula (Hg, Ce)$Sr_{2-x}Ce_xCuO_{4+\delta}$. On the other hand, a pure 1201 phase was identified in system (II), i.e., by introducing lanthanum. The EDS analysis performed on numerous crystals evidenced in fact a small copper excess and a slight cerium deficiency with respect to the nominal composition according to (II), leading to the formulation $Hg_{0.4}Ce_{0.5}Sr_{2-x}La_xCu_{1.1}O_{4+\delta}$ with $0.4 \leq x \leq 0.8$. The electron diffraction study shows the existence of a superstructure. The reconstruction of the reciprocal space evidences a doubling of the b and c parameters, $a = a_p$, $b = 2a_p$, and $c = 2c_{1201}$, and the following conditions of reflection: hkl: $k + l = 2n$ leading to $Ammm$, $A2mm$, $Amm2$, and $A222$ as possible space groups. The [001], [010], and [100] ED patterns of the $x = 0.6$ sample are given as examples in Fig. 1. Note that very weak $hk0$ reflections with $k = 2n + 1$ are observed in the [001] ED

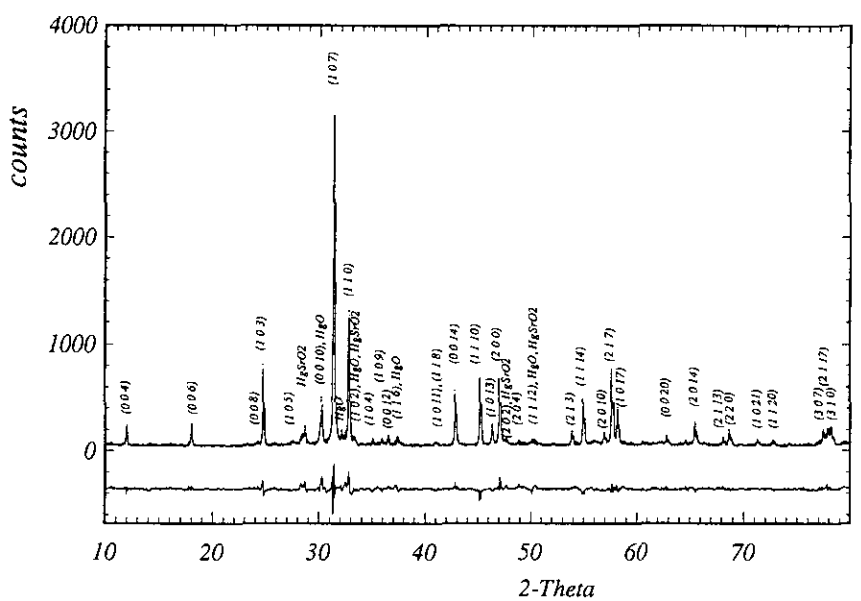

FIG. 2. X ray diffraction patterns (experimental, dotted line; calculated and difference, solid lines) for $Hg_{0.4}Ce_{0.5}Sr_{1.4}La_{0.6}Cu_{1.1}O_{4+\delta}$ with identification of the diffraction peaks.

TABLE 1
Refined Cell Parameters

Cationic actual compositions	a (Å)	b (Å)	c (Å)	V (Å^3)
$Hg_{0.4}Ce_{0.5}Sr_{1.6}La_{0.4}Cu_{1.1}O_{4+\delta}$	3.7326(3)	7.5726(6)	17.9467(7)	507.3
$Hg_{0.4}Ce_{0.5}Sr_{1.4}La_{0.6}Cu_{1.1}O_{4+\delta}$	3.7352(2)	7.5749(3)	17.9657(7)	508.3
$Hg_{0.4}Ce_{0.5}Sr_{1.3}La_{0.7}Cu_{1.1}O_{4+\delta}$	3.7378(2)	7.5697(4)	17.9542(9)	508.0
$Hg_{0.4}Ce_{0.5}Sr_{1.2}La_{0.8}Cu_{1.1}O_{4+\delta}$	3.7384(3)	7.5698(6)	17.9460(9)	507.5

pattern; they result from the presence of defects which will be detailed in the last section.

The XRD patterns can be indexed on the basis of this quadruple cell; an example is given in Fig. 2 for the sample $x = 0.6$. The cell parameters are given in Table 1 for different y and x values. It can be seen that for a given y value, the cell parameters do not vary significantly with x, the variations being vary small so that the cell volume remains approximately constant in agreement with the close ionic radii of lanthanum and strontium.

The HREM study of the composition $Hg_{0.4}Ce_{0.5}Sr_{1.4}La_{0.6}Cu_{1.1}O_{4+\delta}$ ($x = 0.6$) allows the main structural features to be evidenced. The stacking mode of the layers is easily identified from the [010] HREM image (Fig. 3). In this image, the cation positions appear as dark dots. The contrast consists of a group of three staggered dark dots correlated to the heavier atom positions, separated by a row of smaller gray dots correlated to the copper positions. These dots are spaced 3.75 Å along **a** and the periodicity along **c** is about 9 Å. Such a contrast is in agreement with the 1201-type structure (Fig. 4) and the theoretical images previously calculated for the Hg/Pr 1201 cuprate (6). Along that orientation, it is indeed impossible to detect any ordering, in agreement with the ED pattern, since the different cations are projected onto a single point whatever the order. Thus, these images confirm only the 1201 mode of the layer stacking according to the following sequence along **c**: $[(Sr, Ln)O]_\infty$–$[Hg_{1-x}M_xO_\delta]_\infty$–$[(Sr, Ln)O]_\infty$–$[CuO_2]_\infty$.

The origin of the superstructure can be detected on the [100] HREM image. The ordering phenomena are clearly observed in the thicker part of the crystal where the different layers of cations are imaged as dark dots or white dots, depending on the focus value. The identification of the ordered layers is made through the analysis of their contrast in the very thin parts on the crystal's edge and confirmed by the theoretical image calculations. In Fig. 5a, the different layers are easily identified from the contrast of the right part of the image where the cation positions appear as dark dots. The mercury layers run in the middle of a group of three rows of dark dots, two of them being arrowed as examples. Along these rows, parallely to **b**, it appears clearly that a large darker dot alternates

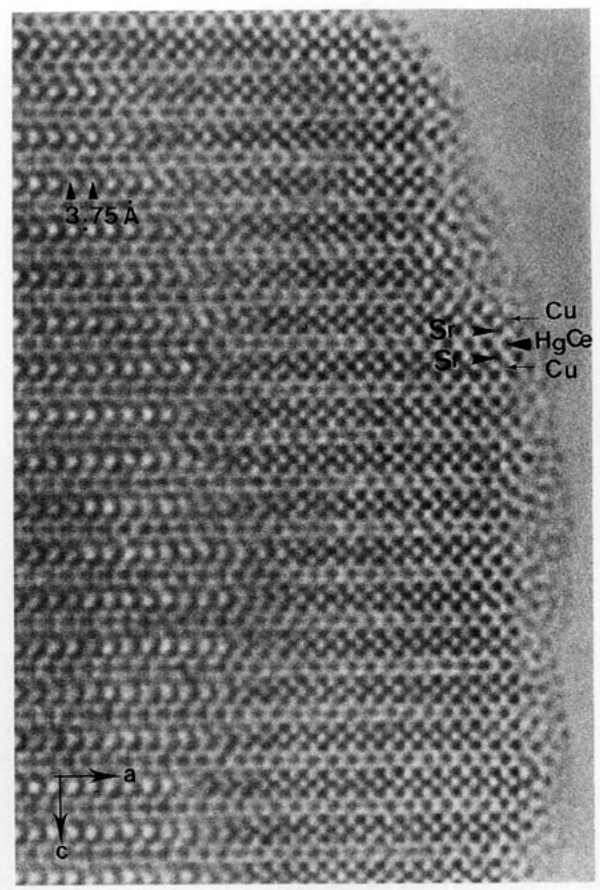

FIG. 3. [010] HREM image for $Hg_{0.4}Ce_{0.5}Sr_{1.4}La_{0.6}Cu_{1.1}O_{4+\delta}$; the cation positions are imaged as dark dots; they are marked on the right side of the micrograph.

with a smaller one in the left part of the image. This means that a 1:1 cation ordering occurs in the mixed layer, i.e., a Hg atom alternates with another M atom. This ordering is translated $b/2 = a_p$ in the adjacent 1201 layer at a distance of 9 Å, involving a centered cell "$2a_p \times 2c_{1201}$," in agreement with the ED pattern symmetry. This image shows also that the mercury layer is the only one which exhibits an ordering phenomenon. At this stage of the observations, it is not possible to determine what kind of M cations are distributed in an ordered way with mercury

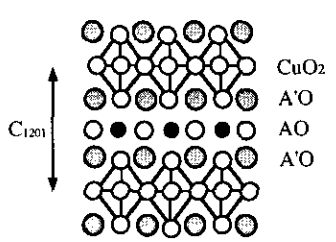

FIG. 4. Idealized drawing of the 1201 AA type structure, $a_2^1CuO_5$, showing the stacking of the layers.

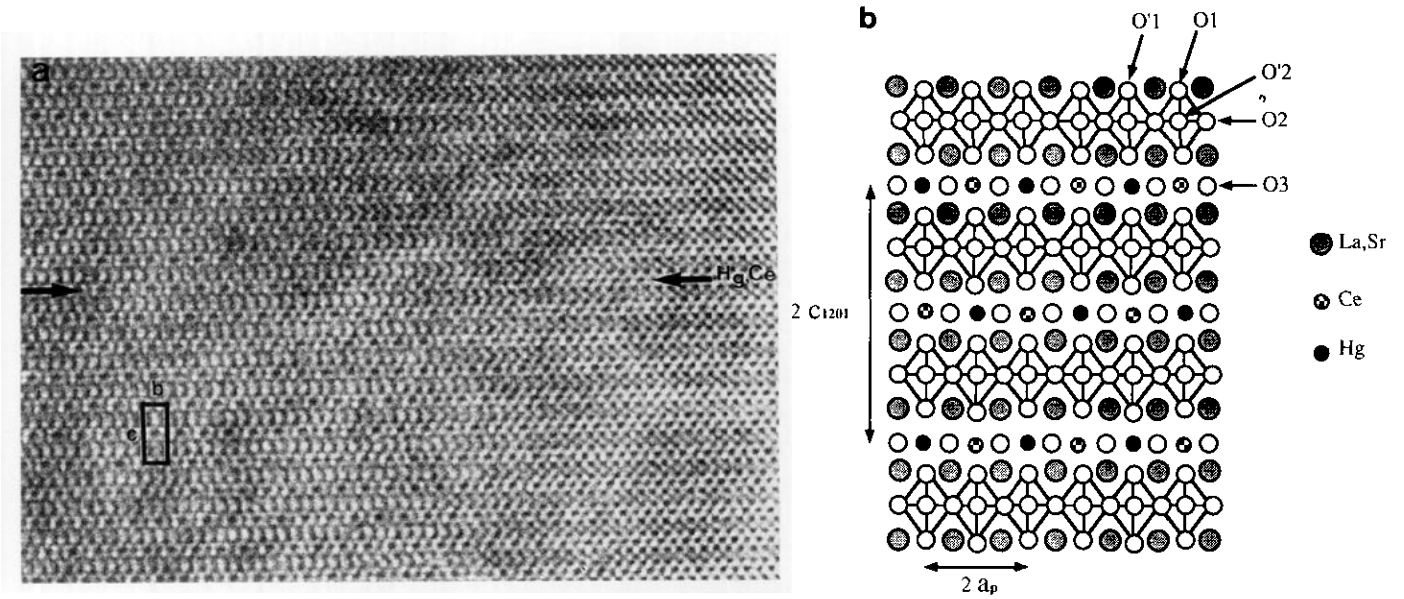

FIG. 5. (a) [100] HREM image for $Hg_{0.4}Ce_{0.5}Sr_{1.4}La_{0.6}Cu_{1.1}O_{4+\delta}$. (b) Schematic projection along **a** of the $a_{1201} \times 2a_{1201} \times 2c_{1201}$ supercell due to ordering between Hg and Ce. The labels for oxygen atoms are those used for the structural study.

within the $[Hg_{1-x}M_xO_\delta]_\infty$ layers: Ce, Cu, La, or Sr. However taking into consideration the previous results observed for the barium mercury cuprates (7, 8), it appears most probable that the excess copper sits on the mercury sites. In the same way, the similarity of cerium and praseodymium suggests that cerium is also located in the mercury layers like in the praseodymium cuprate $Hg_{0.4}Pr_{0.6}Sr_{2-x}Pr_xCuO_{4+\delta}$ (3). Thus in this hypothesis, one cerium row parallel to **a** alternates along **b** with one mercury (copper) row in the $[(Hg_{0.4}Cu_{0.1})Ce_{0.5}O_\delta]_\infty$ layer, whereas lanthanum and strontium are statistically distributed in the adjacent $[Sr_{0.7}La_{0.3}O]_\infty$ layers (Fig. 5b). This is also in agreement with the similar sizes of strontium and lanthanum, which explains why 1201 mercury cuprates involving lanthanum and or strontium on the mercury sites could not be synthesized. Thus the most probable cationic distribution between the copper octahedral layers can be represented by the formula $[Hg_{0.4}Cu_{0.1})Ce_{0.5}]_{ordered}$ $[Sr_{1.4}La_{0.6}]_{stat}$ $CuO_{4+\delta}$. The corresponding simulated images, identical to those of the praseodymium cuprate (6), fit perfectly with the experimental images, strongly supporting this hypothesis.

In order to test this model, calculations have been carried out from powder X ray data assuming *Ammm* as space group. Starting from the classical 1201 structure with an $a_p \times a_p \times c_{1201}$ cell, atom position are calculated for the $a_p \times a_p \times 2c_{1201}$ supercell in order to determine the nature of the different crystallographic sites in the space group *Ammm* (Table 2). Only ordering between mercury (copper) and cerium is considered according to the above distribution. In the studied angular range ($6° \leq 2\theta \leq 80°$), 113 possible reflections are allowed by the space group and are considered in the calculations. On the X ray diffraction pattern (Fig. 2), small extra peaks are detected due to impurities or unreacted phases ($(La, Sr)_2CuO_4$, $SrHgO_2$, CeO_2, $SrCO_3$); they are introduced in the calculations as secondary phases.

In order to limit the number of variables, some assumptions were made during the refinements: $B_{(Hg,Cu)}$ and $B_{(Ce)}$ were refined together with the same value, $B_{(O)}$ was fixed to 1 Å^2, $z(O)_{(1)}$ and $z(O_{(1)})$ were related by the function $z(O'_{(1)}) = z(O_{(1)}) + \frac{1}{2}$ according to the fact that O(1) and O'(1) belong to the same SrO layer (Fig. 5b). After substraction of the background and refinement of the peak profile parameters, positional parameters and isotropic B factors were successively refined allowing the R profile

TABLE 2

Refined Crystal Data Obtained for $Hg_{0.4}Ce_{0.5}Sr_{1.4}La_{1.6}Cu_{1.1}O_5$ (Space Group *Ammm* N°65), a = 3.7352(2) Å, b = 7.5749(3) Å, c = 17.9657(7) Å

Atom	Site	x/a	y/b	z/c	B (Å^2)
Hg, Cu	2a	0	0	0	0.5(1)[a]
Ce	2b	0	1/2	0	0.5(1)[a]
La, Sr	8q	1/2	1/4	0.1477(1)	1.1(1)
Cu	4i	0	0	1/4	1.5(2)
O(1)	4i	0	0	0.1124(8)	1.0[b]
O'(1)	4i	0	0	0.6124(8)	1.0[b]
O(2)	4j	1/2	0	1/4	1.0[b]
O'(2)	4e	0	1/4	1/4	1.0[b]
O(3)	4h	1/2	0.340(3)	0	1.0[b]

[a] Refined with the same value.
[b] Value arbitrarily fixed.

to be lowered to $R_p = 0.089$, $R_{wp} = 0.113$, and $R_i = 0.099$. At this stage, a possible deviation from the O_5 stoichiometry and a splitting of the O(3) oxygens from their ideal positions, due to the size difference between cerium and mercury, were considered. The y variable, initially fixed to $y = \frac{1}{4}$ and the occupancy factor of the 4h site were then refined. They make it possible to decrease the R values to $R_p = 0.080$, $R_{wp} = 0.105$, and $R_i = 0.067$, for $y = 0.340(3)$ and $\tau = 1.00(3)$. This result can be considered significant and shows that, if it exists, the oxygen deficiency is very small, and thus that δ is close to 1.

In order to test the possibility to replace cerium by strontium the hypothetical cationic distribution $[(Hg_{0.4}Cu_{0.1})Sr_{0.5}]_{ordered}[Sr_{0.9}La_{0.6}Ce_{0.5}]_{stat}CuO_5$ has been tested, taking into consideration the fact that a 1:1 ordering occurs between mercury and strontium as observed in the 1201 cuprate $HgBiSr_7SbCu_2O_{15}$ [9]. All the calculations lead to a significant increase of the R factors, $R_p = 0.095$, $R_{wp} = 0.135$, and $R_i = 0.103$, and to a negative B value for the atoms in the mercury layers. On the other hand, the possibility of replacing cerium by lanthanum in these layers, although not very likely, cannot be tested owing to the isoelectronic character of Ce(IV) and La(III).

Thus XRD calculations confirm the ordered cationic distribution deduced from the HREM observations and simulations. Figure 2 shows the agreement between the observed and calculated X ray diffraction patterns. The interatomic distances (Table 3) are similar to those usually observed. Moreover the apical Ce–O distances, close to the Hg–O distances, i.e., 2 Å, confirm that these sites cannot be occupied by larger cations such as strontium or lanthanum. Note that Hg(II) exhibits a dumbbell coordination, whereas cerium is octahedrally coordinated.

TABLE 3
Interatomic Distances, in Å, Calculated for $Hg_{0.4}Ce_{0.5}Sr_{1.4}La_{0.6}Cu_{1.1}O_5$

(Hg/Cu)–O'(1)	2.02(1) × 2
(Hg/Cu)–O(3)	3.18(2) × 4
Ce–O(1)	2.02(1) × 2
Ce–O(3)	2.23(1) × 4
(La/Sr)–O(1)	2.733(6) × 2
(La/Sr)–O'(1)	2.733(6) × 2
(La/Sr)–O(2)	2.636(1) × 2
(La/Sr)–O'(2)	2.618(1) × 2
(La/Sr)–O(3)	2.740(6) × 1
Cu–O(1)	2.47(1) × 1
Cu–O'(1)	2.47(1) × 1
Cu–O(2)	1.868(0) × 2
Cu–O'(2)	1.894(0) × 2

Order–Disorder Phenomena and Extended Defects

The most frequent phenomena which have been observed are the direct consequences of the structural characters of the phases, i.e., the intergrowth of two rock salt layers, one of them being ordered, with a single perovskite layer.

Order–disorder in the mixed layers. Two types of deviations have been observed in the Hg/Ce ordering. The first one retains the nominal stoichiometry and is shown in Fig. 6a; in this image, the copper atoms appear as bright dots and, at the level of the mixed layer, dark dots (Ce) alternate with gray dots (Hg). If the 1:1 ordering is respected along **b**, the shifting along **c** is sometimes absent (adjacent layers indicated by a dark spot and arrowheaded). It results in a local orthorhombic symmetry with $a = a_p$, $b = 2a_p$, and $c = c_{1201}$ (Fig. 6b); this feature corresponds to the local appearance of an orthorhombic

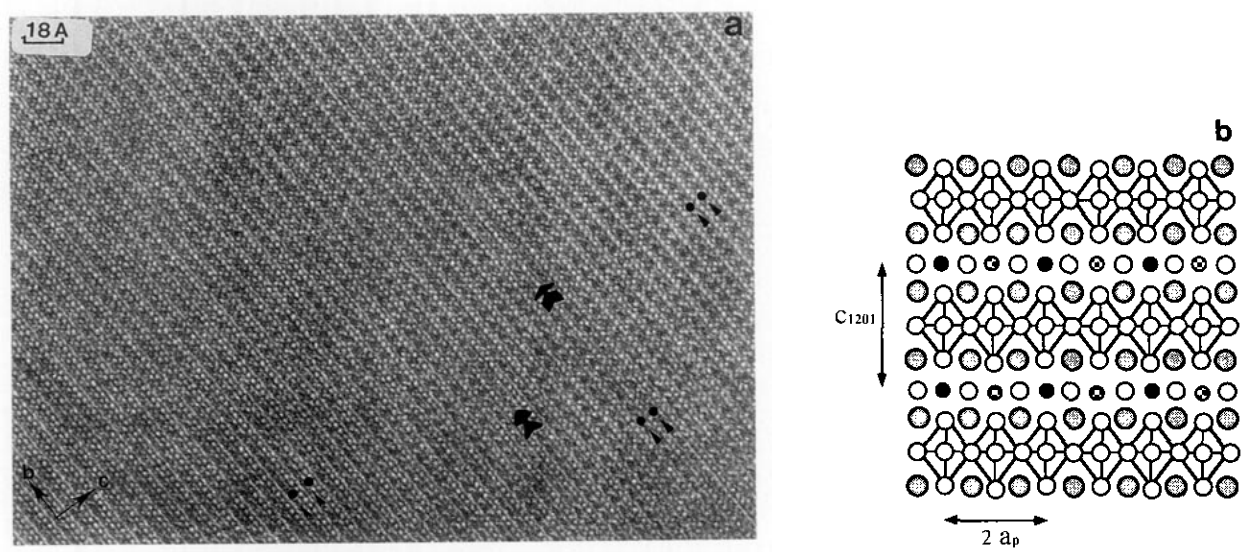

FIG. 6. (a) [100] HREM image showing a variation in the 1:1 ordering: two adjacent 1201 units are no longer translated; they are marked by a dark dot. (b) Idealized drawing of the new supercell: $b = 2a_p$ and $c = c_{1201}$. The symbols for the different atoms are the same as in Fig. 5b.

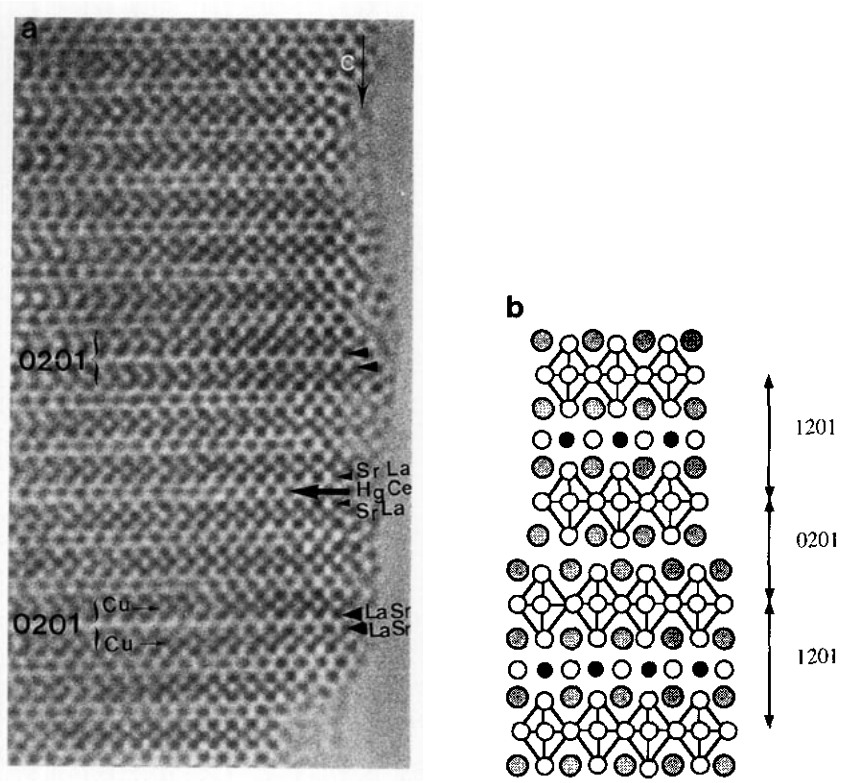

FIG. 7. (a) [010] HREM image where stacking faults are observed; the cation positions are correlated to dark dots. The defective members correspond to 0201's. (b) Idealized drawing of the local intergrowth.

O_I-type ordering [3]. In other parts of the crystal, we can see that the 1:1 ordering is no longer observed; this can arise either along a short distance in a double white single row or in the form of small domains, some 10 Å wide (black arrow). In these areas, a uniform contrast is established, similar to that observed at the level of the mercury atoms. Two possible arrangements of the atoms can explain such a contrast. According to the first one, the ordering occurs along the equivalent perpendicular direction of the perovskite subcell; the second one would correspond to the existence of a mercury-rich area. Since the observation along the [010] direction does not evidence the existence of small ordered areas which would be observed according to the first hypothesis, the existence of mercury-rich areas are more probable.

Stacking fault. Elongation of the reflections and streaking along **c** are sometimes observed in the ED patterns. Two structural features generate such phenomena. When the additional spots of the superstructures are the only elongated reflections, whereas the basic reflections are sharp, as shown in Fig. 1c for example, deviations from the perfect 1:1 ordering must be incriminated. However, both types of reflections are sometimes elongated. The HREM images show that this feature results from the existence of stacking defects, as illustrated in Fig. 7a. The cation positions appear as dark dots and the three [AO] layers of the 1201 structure are easily identified as three rows of staggered dark dots. At the level of the defects we observe only two rows of dark dots, associated

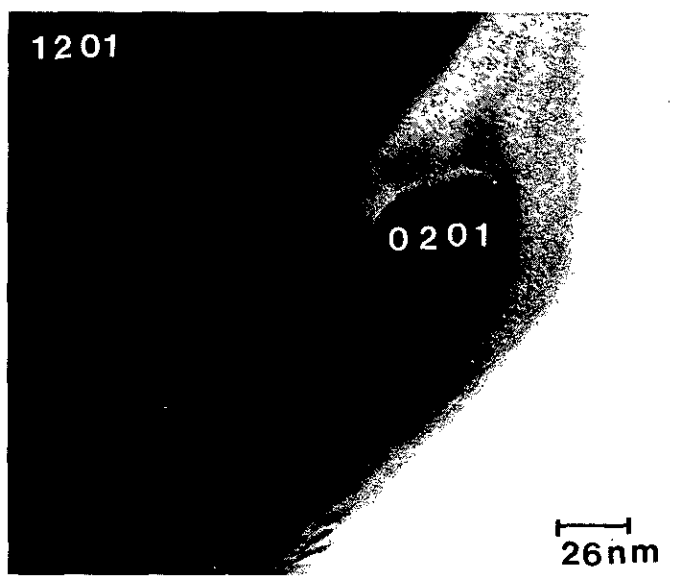

FIG. 8. Low resolution image of a small precipitate of $La_{2-x}Sr_xCuO_4$ in the 1201 matrix.

to two adjacent $[AO]_\infty$ layers building a single rock salt layer; these defective layers result from the local disappearance of the mixed $[Hg_{1-x}M_xO_\delta]_\infty$ layer to form a $La_{2-x}Sr_xCuO_4$ structure (10). Thus, this defective structure can be described from the aleatory intergrowth ($m = n = 1$) of 1201 and 0201 members, according to the general formula $[(Hg_{0.4}Cu_{0.1}Ce_{0.5})(Sr_{2-x}La_x)CuO_{4+\delta}]_m^{1201}$ $[La_{2-x'}Sr_{x'}CuO_4]_n^{0201}$. The schematic drawing of the regular intergrowth $m = n = 1$ is represented in Fig. 7b. The frequency of formation of these defects increases with x.

In the 1201 defective crystals, where 0201 members are locally formed, a sequence of two (or more) adjacent 0201 members is never observed. However, $La_{2-x'}Sr_{x'}CuO_4$ ($m = 0$, $n = \infty$) domains are stabilized in the form of small precipates as shown in Fig. 8; the striking feature is that they are not coherent with the 1201 matrix despite an almost perfect matching of the a and b parameters of the two structures. The EDS analysis confirms the composition of the precipitates but the SAED patterns show that relative orientations of the two species are aleatory.

Antiphase boundaries. Antiphase boundaries are also often observed, as shown in the overall image of Fig. 9a. The enlargement of the thin edge (Fig. 9b) shows that the rows of bright dots in the thicker area are correlated to $[Hg_{1-x}A_xO_\delta]_\infty$ (black arrows) and $[CuO_2]_\infty$ layers (white arrowheads); it appears that, through the boundary, mercury layers are connected to copper layers. At the level of the defect, the framework is strained due to the large difference between the Hg–O and Cu–O apical distances. However, from the schematic drawing of the defect (Fig. 9c), it can be seen that the $[Sr_{1-x}La_xO]_\infty$ layers are not

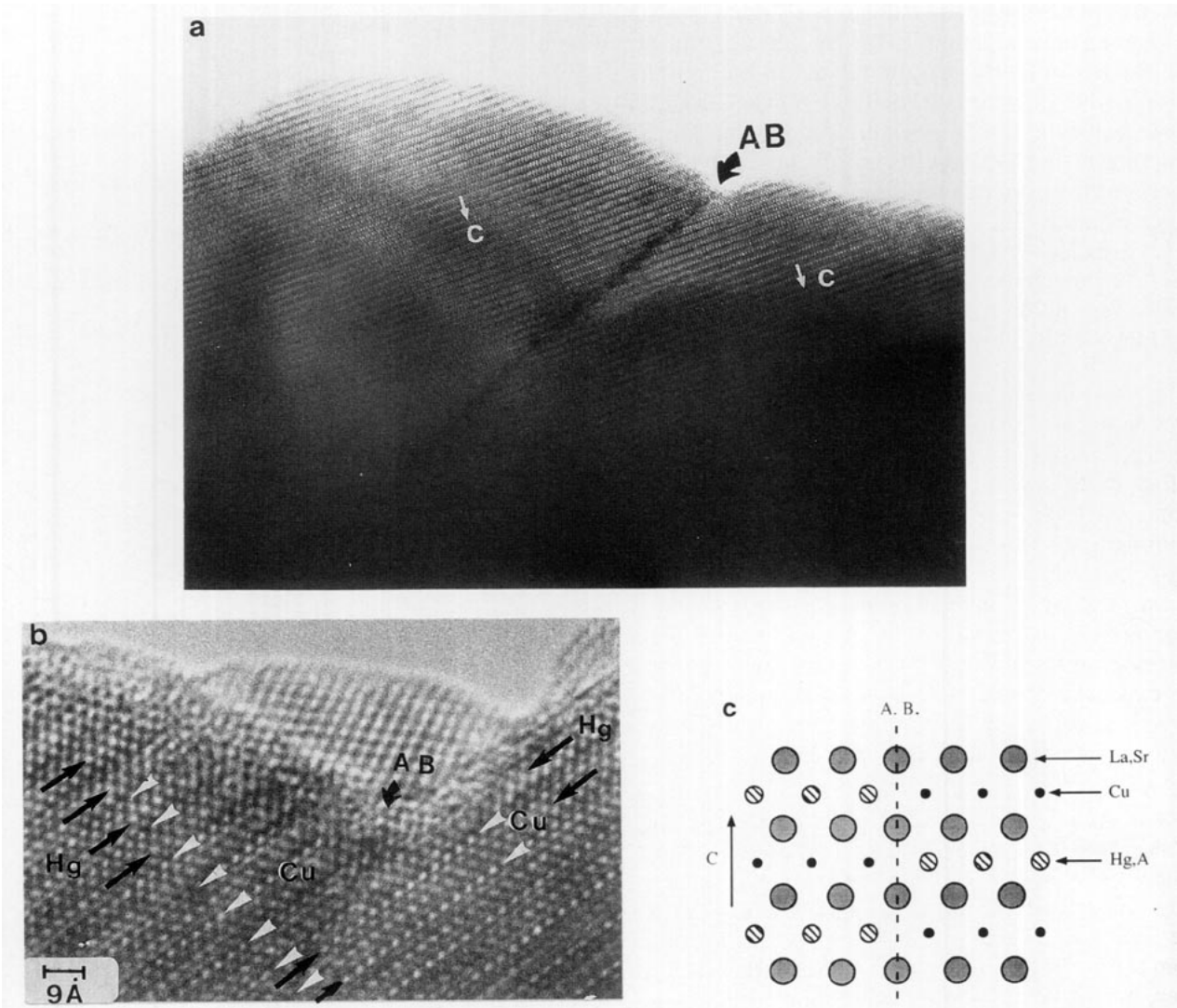

FIG. 9. (a) Example of antiphase boundary (AB). (b) Enlargement of the AB showing the connection of the different layers. Hg/Ce layers are indicated by black arrows and Cu layers by white arrows. (c) Schematic drawing of the defect; only the cationic positions are represented.

interrupted. Numerous examples of shearing mechanisms which involve a similar interconnection of layers of different natures have been recently reported in the bismuth collapsed structures (11, 12) and in the copper oxycarbonates (13); the presence of a small amount of copper in the mixed layer may play a favoring role in the setting up of this structural feature. Note that the junctions of the copper and mercury layers are not ensured in a particular plane as observed in the collapsed phases (Fig. 9a).

CONCLUDING REMARKS

The possibility to stabilize the 1201 structure by cerium in mercury-based cuprates is demonstrated for the first time. In this respect, cerium exhibits a behavior very similar to that of praseodymium (3). It is indeed worth pointing out that all attempts to synthesize 1201 mercury-based cuprates by introducting other lanthanides such as lanthanum or neodymium on the Hg sites were unsuccessful. Such a property may be related to the existence of two possible valencies Pr(III)/Pr(IV) or Ce(III)/Ce(IV) for these elements. It is also remarkable that the 1:1 cationic ordering in the mercury layers of the 1201 cuprates is observed for praseodymium and cerium but not for lead (3) or bismuth (2).

Like the Hg–Pr 1201 cuprates (3), no superconductivity has been detected in the Hg–Ce 1201 phase. This behavior is also very different from the 1212 cuprates of the family $Hg_{0.4}Pr_{0.6}Sr_2Ca_{1-x}Pr_xCu_2O_{6+\delta}$ [4] and $Hg_{0.4}Ce_{0.5}Sr_{2.5}Ca_{0.4}Cu_{2.1}O_{6+\delta}$ (14) that are superconductors with a high diamagnetic volume fraction and a sharp transition at 85 and 51 K respectively.

REFERENCES

1. S. N. Putilin, E. V. Antipov, O. Chmaissen and M. Marezio, *Nature* **362,** 226 (1993).
2. D. Pelloquin, C. Michel, G. Van Tendeloo, A. Maignan, M. Hervieu, and B. Raveau, *Physica C* **214,** 87 (1993).
3. F. Goutenoire, P. Daniel, M. Hervieu, G. Van Tendeloo, C. Michel, A. Maignan, and B. Raveau, *Physica C* **216,** 243 (1993).
4. M. Hervieu, G. Van Tendeloo, A. Maignan, C. Michel, F. Goutenoire, and B. Raveau, *Physica C* **216,** 264 (1993).
5. D. B. Wiles and R. A. Young, *J. Appl. Crystallogr.* **14,** 382 (1981).
6. G. Van Tendeloo, M. Hervieu, X. F. Zhang, and B. Raveau, *J. Solid State Chem.*, in press.
7. J. L. Wagner, P. G. Radaelli, D. G. Hinks, J. D. Jorgensen, J. F. Mitchell, B. Dabrowski, G. S. Knapp, and M. A. Beno, *Physica C* **210,** 447 (1993).
8. A. Maignan, C. Michel, G. Van Tendeloo, M. Hervieu, and B. Raveau, *Physica C* **216,** 1 (1993).
9. D. Pelloquin, M. Hervieu, C. Michel, M. T. Caldès, and B. Raveau, *J. Solid State Chem.* in press.
10. N. Nguyen, J. Choisnet, M. Hervieu, and B. Raveau, *J. Solid State Chem.* **39,** 120 (1981).
11. M. Hervieu, C. Michel, A. Q. Pham, and B. Raveau, *J. Solid State Chem.* **104,** 338 (1993).
12. M. Hervieu, C. Michel, M. T. Caldès, A. Q. Pham, and B. Raveau, *J. Solid State Chem.* **107,** 117 (1993).
13. F. Goutenoire, M. Hervieu, A. Maignan, C. Michel, C. Martin, and B. Raveau, *Physica C* **210,** 359 (1993).
14. A. Maignan, M. Hervieu, C. Martin, C. Michel, and B. Raveau, *Physica C* **232,** 15 (1994).